

Published in final edited form as:

Bone. 2015 April ; 0: 198–207. doi:10.1016/j.bone.2014.12.061.

μ CT-Based, *In Vivo* Dynamic Bone Histomorphometry Allows 3D Evaluation of the Early Responses of Bone Resorption and Formation to PTH and Alendronate Combination Therapy

Chantal M. J. de Bakker, Allison R. Altman, Wei-Ju Tseng, Mary Beth Tribble, Connie Li, Abhishek Chandra, Ling Qin, and X. Sherry Liu*

McKay Orthopaedic Research Laboratory, Department of Orthopaedic Surgery, Perelman School of Medicine, University of Pennsylvania, Philadelphia, PA, United States

Abstract

Current osteoporosis treatments improve bone mass by increasing net bone formation: anti-resorptive drugs such as bisphosphonates block osteoclast activity, while anabolic agents such as parathyroid hormone (PTH) increase bone remodeling, with a greater effect on formation. Although these drugs are widely used, their role in modulating formation and resorption is not fully understood, due in part to technical limitations in the ability to longitudinally assess bone remodeling. Importantly, it is not known whether or not PTH-induced bone formation is independent of resorption, resulting in controversy over the effectiveness of combination therapies that use both PTH and an anti-resorptive. In this study, we developed a μ CT-based, *in vivo* dynamic bone histomorphometry technique for rat tibiae, and applied this method to longitudinally track changes in bone resorption and formation as a result of treatment with alendronate (ALN), PTH, or combination therapy of both PTH and ALN (PTH+ALN). Correlations between our μ CT-based measures of bone formation and measures of bone formation based on calcein-labeled histology ($r = 0.72 - 0.83$) confirm the accuracy of this method. Bone remodeling parameters measured through μ CT-based *in vivo* dynamic bone histomorphometry indicate an increased rate of bone formation in rats treated with PTH and PTH+ALN, together with a decrease in bone resorption measures in rats treated with ALN and PTH+ALN. These results were further supported by traditional histology-based measurements, suggesting that PTH was able to induce bone formation while bone resorption was suppressed.

© 2014 Elsevier Inc. All rights reserved.

*To whom correspondence should be addressed X. Sherry Liu McKay Orthopaedic Research Laboratory Department of Orthopaedic Surgery University of Pennsylvania 426C Stemmler Hall, 36th Street and Hamilton Walk Philadelphia, PA 19104, USA xiaoweil@mail.med.upenn.edu Phone: 1-215-746-4668. (chantald@seas.upenn.edu), (alaltman@mail.med.upenn.edu), (weits@mail.med.upenn.edu), (mtribble@seas.upenn.edu), (connie1@seas.upenn.edu), (abhic@mail.med.upenn.edu), (qinling@mail.med.upenn.edu), (xiaoweil@mail.med.upenn.edu)

Publisher's Disclaimer: This is a PDF file of an unedited manuscript that has been accepted for publication. As a service to our customers we are providing this early version of the manuscript. The manuscript will undergo copyediting, typesetting, and review of the resulting proof before it is published in its final citable form. Please note that during the production process errors may be discovered which could affect the content, and all legal disclaimers that apply to the journal pertain.

6. Conflict of Interest:

Chantal M.J. de Bakker, Allison R. Altman, Wei-Ju Tseng, Mary Beth Tribble, Connie Li, Abhishek Chandra, Ling Qin, and X. Sherry Liu declare that they have no conflict of interest.

Keywords

In vivo μ CT; parathyroid hormone; anti-resorptive treatment; trabecular bone microstructure; bone stiffness; animal models/rodent

1. Introduction

The healthy human skeleton is continuously renewed via coupled and balanced bone remodeling. After menopause, the bone turnover rate accelerates, and bone remodeling is shifted toward a negative balance between bone formation and resorption, resulting in bone loss [1]. Current osteoporosis treatments include anti-catabolic agents, which reduce bone resorption [2, 3], and anabolic agents, which increase bone formation [4]. However, due to coupling of bone resorption and formation, drugs that inhibit resorption often also inhibit formation, and those that increase formation also increase resorption, thereby limiting their potential benefits [2-4]. Recent data suggest that intermittent parathyroid hormone (PTH) treatment, currently the only FDA-approved anabolic agent, may increase bone formation partly through a modeling-based mechanism (bone formation without prior resorption) [5-9]. Therefore, it has been hypothesized that combination therapy of PTH with an anti-catabolic agent could use this modeling-based pathway to concurrently activate new bone formation and block resorption, leading to improved bone quality. In support of this hypothesis, our recent study found that treatment with both PTH and alendronate (ALN), a bisphosphonate, resulted in an improved trabecular structure at the rat proximal tibia beyond what occurred with either treatment alone [10].

However, results from clinical and preclinical studies of combination therapy have been highly variable [11-21], and the ability of PTH treatment to stimulate bone formation while osteoclast resorption is inhibited, remains controversial. This is partly due to technical limitations in the ability to directly assess bone resorption and formation in a simultaneous and longitudinal manner. Although bone formation can be assessed using dynamic histomorphometry with double fluorochrome labeling, this technique is limited by its two-dimensional, destructive nature and its inability to quantify bone resorption. To improve the quantification of bone remodeling, a three-dimensional (3D) dynamic histomorphometry method has been developed that can simultaneously identify bone formation and resorption sites [22-26]. This method gives highly precise morphological measurements of bone formation and can indirectly measure resorption cavities; however, its destructive nature makes it difficult to longitudinally monitor disease progression or drug effects over multiple time points.

The increased availability of *in vivo* micro-computed tomography (μ CT) scanners allows the possibility of quantifying bone formation and resorption in a non-invasive, longitudinal manner. The ability to identify bone remodeling sites using *in vivo* μ CT was first demonstrated by Waarsing *et al.*, who used registered *in vivo* μ CT images to investigate changes in trabecular microarchitecture and qualitatively identify regions of bone remodeling in the rat tibia [27]. More recently, Schulte *et al.* developed an innovative method to longitudinally assess trabecular bone formation and resorption in mouse caudal

vertebrae based on *in vivo* μ CT images [28]. After registering longitudinal μ CT scans from the same animal at two different time points, the two images are superimposed, allowing for measurement of bone remodeling. Resorption is identified as the bone areas only present in the earlier images, while bone formation is identified as the bone areas only present in the later scans. This technique provides accurate quantification of bone remodeling in mouse caudal vertebrae in models of post-menopausal osteoporosis [29] and mechanical loading [28, 30, 31].

Despite the utility of this technique in measuring bone remodeling in the caudal vertebra, the trabecular regions of the tibia, femur, and lumbar spine are more functionally relevant skeletal sites in rodent models of metabolic diseases and drug treatments, and are therefore more commonly used to study bone quality. However, the unclosed growth plate and continuous skeletal growth in the long bones of adult mice and rats significantly affects bone geometry and size over time [27, 33-35]. Although trabecular bone undergoes minimal changes due to longitudinal growth, the dramatic changes that occur in the surrounding cortical bone morphology make it difficult to identify and precisely align the same trabecular bone regions in sequential μ CT scans. For this reason, there is great need for a robust imaging technique that is able to quantitatively track long-bone trabecular remodeling in rodents.

The overall goal of this study was to develop a μ CT-based, 3D *in vivo* dynamic bone histomorphometry technique that would allow us to longitudinally and simultaneously quantify changes in bone formation and resorption in rat tibiae as a result of treatment with ALN, PTH, and combination therapy of both PTH and ALN (PTH+ALN). We validated this novel approach through comparison with standard 2D dynamic bone histomorphometry and a serum resorption marker, and then applied this method to longitudinally track the short-term responses of bone resorption and formation activities to treatment with ALN, PTH, or combination therapy. We hypothesized that adding ALN to PTH treatment would inhibit bone resorption while maintaining the elevated bone formation activities induced by PTH treatment, thus resulting in an additive, beneficial effect on trabecular bone.

2. Materials and Methods

2.1 Animals

A total of 37 three-month-old, female, Sprague Dawley rats were used in this study. Eight rats were excluded due to inadequate image quality caused by motion artifacts during *in vivo* μ CT scans. The remaining 29 rats belonged to 4 treatment groups: PTH (PTH, n=10), alendronate (ALN, n=6), combined PTH and ALN (PTH+ALN, n=6) or vehicle (Veh, n=7). As described in [10], rats in the PTH and PTH+ALN groups were given daily subcutaneous injections of PTH (PTH (1-34), 60 μ g/kg/day dissolved in saline, Bachem, Bubendorf, Switzerland) starting on day 0 for a total of 12 days; rats in the ALN and PTH+ALN groups were given subcutaneous injections of alendronate (alendronate sodium trihydrate, 50 μ g/kg, Sigma Aldrich, St. Louis, MO) every three days starting three days prior to day 0 (day -3) until day 12; and rats in the Veh group were given daily subcutaneous saline injections for 12 days starting from day 0. All rats were sacrificed on day 12. All experiments were approved by the University of Pennsylvania Institutional Animal Care and Use Committee.

2.2 In vivo μ CT Scans

The right proximal tibia of each rat was scanned by μ CT (vivaCT 40, Scanco Medical AG, Brüttisellen, Switzerland) on days 0 and 12 at 10.5 μ m resolution. Rats treated with PTH and PTH+ALN received additional scans on days 4 and 8. A recent study has demonstrated protective effects of PTH treatment against radiation damage [36], and our previous study showed high rates of bone formation in rats treated with PTH despite having received additional scans [10]; thus it is expected that scans on days 4 and 8 had no detrimental effects. As described in [10] and [34], rats were anesthetized (4.0/1.75% isoflurane), and the right leg of each rat was inserted into a custom holder to ensure minimal movement during the scan. A 4 mm region of the tibia distal to the proximal growth plate was scanned at 10.5 μ m resolution, 55 keV energy, 145 μ A intensity, 200 ms integration time, and 1000 projections, using a 0.5mm Al filter and a standard, manufacturer-provided beam-hardening correction algorithm, resulting in a total scan time of about 20 minutes and approximate radiation dose of 0.307 Gy per scan. A subset of rats (n=18: PTH: 6, PTH+ALN: 5; ALN: 4, Veh: 3) was also scanned eight days prior to treatment (day -8) to allow for pretreatment measures.

2.3 Registration between Baseline and Follow-up Scans

For each rat, the day 0 and day 12 scans were aligned using linear, mutual-information-based registration software (ITK, NLM) [34, 37]. For the subset of rats also scanned on day -8, the same trabecular volume was aligned in the scans made at day -8, day 0 and day 12 (Fig. 1). This image registration scheme allowed the same volume of trabecular bone to be followed over time so that local instances of bone formation and resorption could be identified within the subvolume.

In each set of sequential images, trabeculae were aligned precisely using a three-step registration procedure: First, baseline (**b**, day 0) and follow-up (**f**, day 12) scans were registered to derive a transformation matrix \mathbf{T}_1 by aligning the cortical bone in each image. After this step, the two images (**b** and \mathbf{f}^1 ; $\mathbf{f}^1 = \mathbf{T}_1\mathbf{f}$) were oriented approximately the same way, but, due to linear growth, the trabecular compartments were offset from each other [34] (Fig. 2A). To eliminate this offset, a landmark-initialized registration of the trabecular compartment (excluding the cortical bone) was performed to more precisely align the trabecular structures (Fig. 2B) and to derive a second transformation matrix \mathbf{T}_2 . Finally, a 146x146x96 voxel trabecular volume of interest (VOI) in the secondary spongiosa starting 2.5 mm distal to the proximal growth plate and spanning to 3.5 mm distal to the growth plate was identified in the baseline scan and extracted from the two images (**b** and \mathbf{f}^2 , $\mathbf{f}^2 = \mathbf{T}_2\mathbf{f}^1$), and was registered to align individual trabecular structures within the VOI. Therefore, a third transformation matrix \mathbf{T}_3 was derived. At each step, a visual inspection of the registration result was performed to prevent misalignment caused by local optima of the registration algorithm. Transformation matrices of the three, sequential registration steps were then combined to derive the overall transformation matrix \mathbf{T} ($\mathbf{T} = \mathbf{T}_3\mathbf{T}_2\mathbf{T}_1$).

In the traditional image registration scheme, a transformation is applied to the follow-up image (moving image) to match with the baseline image (fixed image). However, transformation of an image inherently causes a certain amount of resampling error, resulting

in a difference in image quality between the fixed image and the moving image. In order to eliminate such a difference, we developed a new image registration scheme, where \mathbf{T} was divided equally so that one half of the rotation, \mathbf{T}_a was applied to the follow-up image (\mathbf{f}) while the inverse of half of the rotation \mathbf{T}_b ($\mathbf{T}_b = \mathbf{T}_a^{-1}$) was applied to the baseline image (\mathbf{b}). Thus, a single transformation was applied to both the baseline and follow-up images so that they were aligned in a new coordinate system. This technique minimized unequal resampling artifacts between scans (data not shown).

2.4 3D in vivo dynamic bone histomorphometry measurements

Registered and transformed images were Gaussian filtered ($\sigma=1.2$, $\text{support}=2$) and a global threshold (545 mgHA/cm^3 , as determined based on previous data [10]) was applied to delineate bone voxels from the bone marrow and background. The resulting binarized images were then analyzed using a custom MATLAB script. Resorbed bone was defined as all bone voxels that were present at the first time point but absent at the second, while formed bone was defined as bone voxels that were present at the second time point, but absent at the first. This resulted in a map indicating the spatial locations of bone formation and resorption sites. To prevent the incorrect labeling of small regions of bone formation/resorption due to slight registration errors or differences in segmentation caused by the partial volume effect, the surface layer of all bone formation and resorption areas was excluded from analysis. This minimized error and resulted in a more conservative measure of bone formation and resorption.

The resulting map of bone formation and resorption was then used to obtain 3D measurements of the volume, thickness, and surface area of bone remodeling sites. Specifically, measurements of bone formation were made analogously to standard dynamic bone histomorphometry and were calculated as follows:

$$\text{Bone formation rate (BFR/BS)} = \frac{\text{volume of formed bone}}{(\# \text{ of days}) \cdot (\text{total bone surface area})} \quad (\text{a})$$

$$\text{Mineral apposition rate (MAR)} = \frac{\text{thickness of formed bone}}{\# \text{ of days}} \quad (\text{b})$$

$$\text{Mineralizing surface (MS/BS)} = \frac{\text{surface area of formed bone}}{\text{total bone surface area}} \quad (\text{c})$$

Bone resorption was quantified similarly:

$$\text{Bone resorption rate (BRR/BS)} = \frac{\text{volume of resorbed bone}}{(\# \text{ of days}) \cdot (\text{total bone surface area})} \quad (\text{d})$$

$$\text{Mineral erosion rate (MER)} = \frac{\text{thickness of resorbed bone}}{\# \text{ of days}} \quad (\text{e})$$

$$\text{Eroding surface } (ES/BS) = \frac{\text{surface area of resorbed bone}}{\text{total bone surface area}} \quad (f)$$

Where surface area was quantified by extracting triangulated surfaces from the map of bone formation and resorption sites using a custom MATLAB script, and thickness was calculated through a distance transformation algorithm included in the scanner software (Scanco Medical). Accuracy of the *in vivo* dynamic histomorphometry measurements was determined by correlation to traditional dynamic histomorphometry (BFR/BS, MAR, MS/BS) and a serum resorption marker (TRAP).

2.5 2D static and dynamic bone histomorphometry

The right tibiae of a subset of rats (n=28: PTH: 8; PTH+ALN: 9; ALN: 5; Veh: 6) were harvested immediately after euthanasia on day 12. Tibiae were embedded in methylmethacrylate (MMA), and a Polycut-S motorized microtome (Reichert, Heidelberg, Germany) was used to cut 5 µm-thick sections for static histology. Sections were stained with Goldner's trichrome to allow for measurement of the number of osteoblasts (Ob.N/BS), number of osteoclasts (Oc.N/BS), osteoblast surface (Ob.S/BS), and osteoclast surface (Oc.S/BS) in the secondary spongiosa (2.0-5.0 mm below the growth plate).

Two days and nine days prior to sacrifice (days 3 and 10), 16 rats received subcutaneous injections of calcein (15 mg/kg, Sigma Aldrich, St. Louis, MO) to allow for histological measures of bone formation. 8 µm-thick sections were cut from the MMA-embedded tibiae and dynamic histomorphometry measurements of bone formation rate (BFR/BS), mineral apposition rate (MAR), and mineralizing surface (MS/BS) were made in the secondary spongiosa based on the calcein labels. The 3D *in vivo* dynamic histomorphometry measurements were then correlated with the standard 2D measurements for validation. All measurements were made using Bioquant Osteo Software (Bioquant Image Analysis, Nashville, TN). A qualitative comparison was also made between bone formation identified in each 2D histology section and the corresponding µCT cross-section. 2D histology slides and 3D µCT images were aligned through an image registration procedure where the MMA-embedded bone (from which the histology cross-section had been cut) was scanned and registered to the *in vivo* µCT scan, allowing for identification of the precise cut-plane from which the 2D histology images had been generated.

2.6 Serum Biochemistry Analysis

At sacrifice, blood was collected via cardiac puncture for a subset of rats (n=3 in each group). The serum was removed and serum levels of the resorption marker TRAcP 5b (TRAP) were measured (RatTRAP™ Assay, Immunodiagnostic Systems, Scottsdale, AZ).

2.7 Micro Finite Element Analysis (µFEA)

Bone stiffness within each registered trabecular VOI was determined through micro-finite element analysis (µFEA). Each voxel in the registered, binarized subvolume was converted to an eight-node brick element, and bone tissue was modeled as an isotropic, linear elastic material with a Young's modulus (E) of 15 GPa and a Poisson's ratio of 0.3 [38]. A 0.01 mm

displacement was applied along the axial direction of the bone to model a uniaxial compression test, and the reaction force was calculated using an element-by-element pre-conditioned conjugate gradient solver [39]. Trabecular bone stiffness was then calculated by dividing the reaction force by the applied displacement.

2.8 Statistical Analysis

Bone remodeling parameters based on 3D *in vivo* dynamic bone histomorphometry measured after 12 days of treatment were compared among the 4 treatment groups using analysis of variance (ANOVA). Additionally, for a subset of specimens, longitudinal comparisons were made to assess changes in bone remodeling parameters before and after treatment using a twoway, repeated-measures ANOVA, covaried by the baseline measures. Bonferroni corrections were applied to all *post-hoc* tests. Bone remodeling parameters measured based on 3D *in vivo* dynamic bone histomorphometry were correlated to bone formation measures made based on traditional, calcein-labeled histology, and to serum TRAP using linear regression. All statistical analyses were performed using NCSS 7.1.14 (NCSS, LLC, Kaysville, UT). Statistical significance was defined as $p < 0.05$, and error bars represent the standard error of the mean (SEM).

3. Results

3.1 3D registration and linear growth in rat tibiae

The registration process developed in this study resulted in an accurate alignment of trabeculae in the secondary spongiosa (Fig. 1). Although the rats used in this experiment were skeletally mature, they continued to experience linear growth due to the unclosed growth plate. As shown in Fig. 2, this resulted in distinct changes in cortical bone morphology. To exclude the effects of cortical bone growth, a VOI was selected that only included a trabecular subvolume.

3.2 Validation of 3D *in vivo* dynamic bone histomorphometry measurements

Although it is challenging to locate exactly the same cross-section from the 3D *in vivo* dynamic image and the 2D calcein-labeled histology slide due to their different slice thickness (10.5 μm vs. 8 μm), the 2D, calcein-labeled histology slides in general yielded a good agreement with the corresponding, registered slices from the 3D *in vivo* dynamic image for all 4 treatment groups (Fig. 3). Particularly, the endosteal bone formation identified through μCT very closely matches the double-labeled endosteal surface on the histology slides. Additionally, periosteal bone resorption identified through μCT agrees very closely with regions in the histology slide exhibiting a scalloped surface, which is indicative of bone resorption. Additionally, μCT -based measures of BFR/BS, MAR, and MS/BS correlated strongly with analogous measures based on traditional dynamic histomorphometry ($r = 0.83, 0.72, \text{ and } 0.78$, respectively, Fig. 3). Because it is not possible to obtain quantitative measures of bone resorption through traditional dynamic histomorphometry, measurements of the serum resorption marker TRAP were used to assess the ability of *in vivo* dynamic bone histomorphometry to measure bone resorption. There was a strong correlation between μCT -based BRR/BS and serum TRAP ($r = 0.94$, Fig. 3).

3.3 Cross-sectional comparison of bone structure and dynamic parameters in response to treatments

After 12 days of treatment, the bone volume fraction (BV/TV) of rats treated with PTH+ALN was 83% greater than that of the Veh group and 50% greater than that of ALN-treated rats (Fig. 4). Additionally, trabecular stiffness of rats treated with PTH+ALN was 174% greater than that of Veh-treated rats.

BFR/BS was not significantly different between PTH- and PTH+ALN-treated rats and was also not significantly different between rats treated with ALN and those treated with Veh (Fig. 4). Rats treated with PTH showed 514% greater BFR/BS and rats treated with PTH+ALN showed 602% greater BFR/BS than those treated with Veh. Additionally, rats treated with PTH+ALN had an 82% lower BRR/BS than those treated with Veh and 76% lower BRR/BS than those treated with PTH, while rats treated with ALN tended to have a 62% lower BRR/BS than Veh-treated rats ($p=0.059$). μ CT-based measurements of MAR, MS/BS, MER, and ES/BS provide further insight into these differences in bone formation and resorption rates: Rats treated with PTH+ALN showed no significant difference in MAR and MS/BS from those treated with PTH, and there was no difference between Veh- and ALN-treated rats in MAR and MS/BS. PTH-treated rats had a 41% greater MAR and 273% greater MS/BS than Veh-treated rats, and similarly, rats treated with PTH+ALN had a 37% greater MAR and 344% greater MS/BS than those treated with Veh. In contrast, rats treated with ALN and PTH+ALN had a 22% and 27% lower MER, respectively, than those treated with Veh, while the MER of PTH-treated rats was not significantly different from that of Veh-treated rats. PTH+ALN-treated rats had a 72% lower ES/BS than did rats treated with Veh and had a 56% lower ES/BS than those treated with PTH. Veh-treated rats had a greater ES/BS than all other treatment groups.

3.4 Longitudinal changes in bone structure and dynamic parameters in response to treatments

Standard measures of BV/TV and trabecular stiffness increased 28% and 49%, respectively, in rats treated with PTH, and BV/TV and trabecular stiffness underwent a 45% and 108% increase, respectively, in PTH+ALN-treated rats over the 12-day treatment period (Fig. 5). Rats treated with Veh and ALN, on the other hand, underwent no significant changes in BV/TV or trabecular stiffness over the treatment period (Fig. 5).

In addition to scans before and after treatment, a subset of rats was also scanned eight days prior to the start of treatment, allowing for a baseline measure of bone remodeling. This allowed for additional, longitudinal assessments of changes in bone remodeling in each rat (Fig. 5). In rats treated with PTH, BFR/BS increased 237% and MS/BS increased 190% as a result of treatment. Similarly, PTH+ALN-treated rats underwent a 331% increase in BFR/BS and a 277% increase in MS/BS. On the other hand, rats treated with Veh and ALN showed no significant change in BFR/BS or MS/BS over the treatment period. Meanwhile, rats treated with ALN and PTH+ALN showed a 66% and 81% decrease in BRR/BS, respectively, and rats treated with PTH+ALN had a 68% decrease in ES/BS, while Veh- and PTH-treated rats underwent no significant change in BRR/BS or ES/BS over time. MER decreased over the course of the experiment for all treatment groups, and MAR decreased

35% in rats treated with Veh and ALN, and tended to undergo an 8% decrease in rats treated with PTH+ALN ($p=0.067$).

3.5 Cross-sectional Comparisons of 2D static and dynamic bone histomorphometry measurements in response to treatments

Traditional static bone histomorphometry indicates that PTH-treated rats had 69% greater Ob.N/BS than those treated with Veh and 170% greater Ob.N/BS than ALN-treated rats (Table 1). Additionally, Ob.N/BS tended to be 82% greater for rats treated with PTH+ALN than for those treated with ALN ($p=0.095$). Rats treated with PTH showed 107% greater Ob.S/BS, and rats treated with PTH+ALN showed 99% greater Ob.S/BS than those treated with Veh. There was no difference between PTH- and PTH+ALN-treated rats in Ob.S/BS, and similarly no significant difference was found between Veh- and ALN-treated rats. Rats treated with ALN and PTH+ALN had 55% and 46% lower Oc.N/BS, respectively, than those treated with PTH, and rats treated with ALN tended to have 52% lower Oc.N/BS than Veh-treated rats ($p=0.062$). No significant differences among treatment groups were found in Oc.S/BS. Histology-based BFR/BS was 345% and 267% greater in rats treated with PTH and PTH+ALN, respectively, than in Veh-treated rats. Similarly, histology-based MAR and MS/BS were also greater for rats treated with PTH and PTH+ALN than for Veh- and ALN-treated rats.

4. Discussion

The *in vivo* dynamic bone histomorphometry technique developed in this study allowed for a quantitative, longitudinal assessment of the effects of osteoporosis treatments on trabecular bone remodeling in rat long bones. The accuracy of this novel method was supported by the strong correlations between μ CT-based and traditional measures of bone remodeling, and the qualitative agreement between μ CT- and histology-based localization of bone formation sites (Fig. 3). Application of this technique resulted in a non-invasive, 3D evaluation of the bone formation and resorption events taking place as a result of treatment with PTH, ALN, or combined PTH+ALN. Additionally, the longitudinal nature of this method enables pre-treatment measurements, allowing each rat to serve as its own control.

Similar to studies of trabecular remodeling in caudal vertebrae [28-31], the *in vivo* dynamic histomorphometry method described here results in longitudinal measures of both bone formation and resorption, allowing the bone modeling and remodeling mechanisms behind changes in trabecular structure to be investigated. Correlation coefficients between histology- and μ CT-derived MAR and MS/BS were highly consistent between this study and that of Schulte *et al.* [28], indicating a similar accuracy relative to traditional dynamic histology. However, in contrast to previous studies of caudal vertebrae [28-31], the registration process utilized in this study was further complicated by the presence of linear growth in the tibia. Linear growth due to the unclosed growth plate makes it challenging to precisely align the trabecular compartment of rodent long bones, as the cortical and trabecular compartments do not grow in the same way [34, 35]. To our knowledge, there have been no previous μ CT-based measurements of bone remodeling made in the trabecular compartment of long bones. Through our novel, three-step registration procedure, we were

able to delineate bone changes due to trabecular remodeling from those due to linear growth (Fig. 2). This resulted in a highly accurate, precise alignment of the trabecular structures, and made it possible to identify resorption and formation on the trabecular bone surfaces.

Qualitative comparison between the results of our μ CT-based method and calcein-labeled histology indicates good spatial agreement between regions labeled as bone formation in the histology slides and in the μ CT images, particularly on the endosteal surfaces of the bone (Fig 3). However, a direct comparison of individual trabeculae indicates that disparities in the trabecular bone formation identified through the two different methods do exist. This is caused in part by the difficulty in identifying the precise slice in the 3D μ CT image stack that corresponds to the 2D histology cross-section, due to their different slice thicknesses (10.5 μ m vs. 8 μ m). However, good overall agreement between μ CT- and histology-based identification of bone formation sites and good correlation between these two measures demonstrate that the *in vivo* dynamic bone histomorphometry technique provides a reliable overall assessment of bone formation within the subvolume.

Despite the high correlation between μ CT- and histology-based measures of bone formation, μ CT-based BFR/BS and MS/BS were consistently higher, and MAR was consistently lower, than corresponding histology-based measures. This was likely due to inherent differences in the way these measures were calculated. When calculated through our μ CT-based method, each measure of bone formation is defined directly based on the 3D μ CT volumes that are analyzed. In contrast, the traditional, histology-based method estimates all measurements based on a 2D cross-section of calcein labels that are injected at two discrete time points [40]. Histology-based MAR is based solely on the double-labeled surfaces, meaning that any bone formation occurring after the first calcein injection is not included in this measure of MAR. This could cause an over-estimate relative to μ CT-based MAR, which measures the thickness of all bone formation sites, thus including newly formed, and therefore thinner, areas of bone formation. Similarly, histology-based MS/BS gives a higher weight to double-labeled regions, whereas μ CT-based MS/BS calculates the surface area of bone formation based on all regions of new bone. Thus μ CT-based MS/BS is expected to be greater than that based on histology. Considering these discrepancies, it may be expected that μ CT- and histology-based measures of bone formation have varying absolute values. However, the correlation between the measures indicates that the μ CT-based method provides reliable quantification of bone remodeling.

Consistent with our previous findings [10], the current study showed an improved trabecular structure based on analysis of a trabecular sub-volume in rats treated with PTH and PTH +ALN. This is supported by *in vivo* dynamic bone histomorphometry measurements, which show greater bone formation measures (BFR/BS, MAR, MS/BS) in all groups treated with PTH, together with lower bone resorption (BRR/BS, MER, ES/BS) in ALN-treated groups. These μ CT-derived measures were further supported by measurements of osteoclast and osteoblast cell counts, and are in agreement with measures of bone formation based on calcein-labeled histomorphometry. Taken together, high rates of formation (as measured by BFR/BS, MAR, MS/BS, and Ob.S/BS) and concurrent low bone resorption (as measured by BRR/BS, MER, ES/BS, and Oc.N/BS) in PTH+ALN-treated rats indicate that the combination therapy has an additive effect on bone remodeling, as the combination

treatment group was the only group to show both elevated bone formation and low resorption. Additionally, the persistently elevated bone formation even in the presence of low bone resorption in rats treated with PTH+ALN suggests that PTH may act through a resorption-independent mechanism. This supports previous studies which have suggested that PTH induces modeling-based formation, bone formation without prior resorption [5-9], and provides insight into the mechanism behind the additive effect of combination therapy found in our previous study [10].

Earlier studies assessing the effect of PTH and anti-catabolic co-treatment on bone remodeling using traditional histology and serum formation and resorption markers have drawn various conclusions [7-9, 11, 12, 14, 15, 20, 41-44]. Multiple clinical and pre-clinical studies found that groups treated with PTH and ALN had lower levels of serum markers of both resorption and formation than those treated with PTH alone [9, 11, 14, 15, 41, 44]. In contrast to this, when investigating the co-treatment of PTH and anti-resorptive agents ALN and osteoprotegerin (OPG) in ovariectomized mice, Samadfam *et al.* [43] found that osteoblast number and activity were similar in mice treated with PTH and combination therapy of PTH+ALN, while osteoclast activity was reduced in PTH+ALN-treated mice as compared to those treated with PTH alone. Meanwhile, Ma *et al.* [42] found similar elevations in bone formation (BFR, MAR, activation frequency) in PTH-treated rats that had been pre-treated with ALN, Raloxifene, or estrogen compared to PTH-treated rats that had not received pre-treatment. Finally, using a unique fluorescent labeling regimen, Lindsay *et al.* [8] quantified remodeling- and modeling-based formation in patients following a one-month treatment with PTH. Results from this study indicated a greater amount of modeling-based bone formation in patients treated with PTH compared to controls, suggesting that PTH-induced bone formation may be partially uncoupled from prior resorption [8]. The wide variety of conclusions drawn by these studies may be due in part to variations in the duration of therapy, as the anabolic effects of PTH treatment are known to decrease with extended treatment times [45]. The design of the current study only consists of a 12-day treatment period for rats; thus it reflects early bone dynamic responses to PTH, ALN, and combination therapies.

The longitudinal design of this study allowed bone remodeling to be compared before and after treatment within the same rat (Fig. 1), providing direct assessment of the bone remodeling response to each treatment. Similar to the cross-sectional comparisons, longitudinal analyses again confirm the additive effect of combination therapy over monotherapy and again show an increase in bone formation with a concurrent decrease in bone resorption in PTH+ALN-treated rats. Although results follow consistent trends, longitudinal comparison of MAR and MER shows that both decrease over the course of the experiment in vehicle-treated rats. While this effect may be due to the natural slowing of bone turnover with growth, it may also be due to a limitation in the design of this study. Namely, bone remodeling was assessed over an 8-day period prior to treatment, while it was assessed over a 12-day period during treatment. Because of the finite resolution of the μ CT image, it is possible that the difference in the thickness of bone remodeling sites after 8 vs. 12 days is not measurable (i.e., thickness of bone formation or resorption occurring over a 4-day period was lower than the resolution of the image). Therefore, when this thickness value

was divided by the number of days to obtain a measure of MAR and MER, it appeared as though the rate of mineral apposition or erosion decreased in the vehicle group. It is therefore recommended that the time between scans be kept consistent when using *in vivo* dynamic bone histomorphometry to obtain longitudinal measures of bone remodeling in future studies. However, all groups in this study were scanned following the same schedule; therefore, comparisons among treatment groups remain valid.

Another limitation of this study is the use of young, intact rats: although 3-month-old rats are skeletally mature, their relatively young age suggests that they may not be representative of an osteoporotic patient. Our ongoing follow-up study is to confirm the effects of PTH, ALN, and combination therapy on bone remodeling in an aged, ovariectomized rat model. Additionally, radiation exposure is a concern in any longitudinal, μ CT-based study. However, the radiation dose was relatively low (about 0.307 Gy/scan), and was localized to the tibial metaphysis. Furthermore, it has been shown that weekly μ CT scans have no adverse effect on the proximal tibiae of rats [10, 46], and PTH treatment has been demonstrated to exert a protective effect on bone [36], allowing for frequent scanning.

A unique strength of the current study is the application of a robust registration procedure that can delineate bone changes due to bone modeling (linear growth) and bone remodeling (local bone resorption and formation). For the purpose of this study, we only focused on the local changes on a fixed trabecular subvolume. However, newly generated bone tissue from the growth plate and the distance by which the existing bone tissue “flows away” from the growth plate can be interesting and important parameters for studies of bone modeling [47, 48]. Due to the fact that rodents have continuous longitudinal growth throughout their life, it should be noted that the rate at which the trabecular bone flows away from the growth plate limits the timespan over which a given trabecular volume of interest (VOI) can be followed. For example, 1-month-old rats have a proximal tibial growth rate as fast as 0.31 mm/day (unpublished data), making it difficult to trace a trabecular bone sub-volume for longer than a week. In contrast, the 3-month-old rats used in the current study have a much slower growth rate (1.99 mm proximal tibial growth over 10 weeks, equaling to 0.03 mm/day), thus allowing for a long-term longitudinal follow-up study.

Overall, this study developed and validated a novel, *in vivo* dynamic bone histomorphometry technique that allows longitudinal, 3D measurement of trabecular remodeling in long bones. Application of this technique provides tremendous potential for dissecting changes in bone remodeling induced by treatments and disease states. By tracking the effects of PTH, ALN, and combined PTH+ALN treatment on bone formation and resorption in rat tibiae, we demonstrated that rats treated with PTH+ALN exhibit both an increased bone formation and a decreased bone resorption rate, relative to vehicle-treated controls, suggesting that intermittent PTH may act partially through a modeling-based mechanism.

Acknowledgements

This study was supported by McCabe Pilot Award (to XSL), NIH/NIAMS R03-AR065145 (to XSL), American Society of Bone and Mineral Research (ASBMR) Junior Faculty Osteoporosis Basic Research Award (to LQ), NIH/NIDDK R01-DK09580301 (to LQ), NIH/NIAMS T32-AR007132 (to CMJdB), National Science Foundation

Graduate Research Fellowship (to CMJdB) and Penn Center for Musculoskeletal Disorders (PCMD; NIH/NIAMS P30-AR050950).

References

1. Kushida K, Takahashi M, Kawana K, Inoue T. Comparison of markers for bone formation and resorption in premenopausal and postmenopausal subjects, and osteoporosis patients. *J Clin Endocrinol Metab.* 1995; 80:2447–50. [PubMed: 7629240]
2. Liberman UA, Weiss SR, Broll J, Minne HW, Quan H, Bell NH, Rodriguez-Portales J, Downs RW Jr, Dequeker J, Favus M. Effect of oral alendronate on bone mineral density and the incidence of fractures in postmenopausal osteoporosis. The Alendronate Phase III Osteoporosis Treatment Study Group. *N Engl J Med.* 1995; 333:1437–43. [PubMed: 7477143]
3. Rodan GA, Fleisch HA. Bisphosphonates: mechanisms of action. *J Clin Invest.* 1996; 97:2692–6. [PubMed: 8675678]
4. Goltzman D. Studies on the mechanisms of the skeletal anabolic action of endogenous and exogenous parathyroid hormone. *Arch Biochem Biophys.* 2008; 473:218–24. [PubMed: 18358824]
5. Cusano NE, Bilezikian JP. Combination antiresorptive and osteoanabolic therapy for osteoporosis: we are not there yet. *Curr Med Res Opin.* 2011; 27:1705–7. [PubMed: 21740288]
6. Jilka RL, O'Brien CA, Bartell SM, Weinstein RS, Manolagas SC. Continuous elevation of PTH increases the number of osteoblasts via both osteoclast-dependent and -independent mechanisms. *J Bone Miner Res.* 2010; 25:2427–37. [PubMed: 20533302]
7. Kostenuik PJ, Capparelli C, Morony S, Adamu S, Shimamoto G, Shen V, Lacey DL, Dunstan CR. OPG and PTH-(1-34) have additive effects on bone density and mechanical strength in osteopenic ovariectomized rats. *Endocrinology.* 2001; 142:4295–304. [PubMed: 11564687]
8. Lindsay R, Cosman F, Zhou H, Bostrom MP, Shen VW, Cruz JD, Nieves JW, Dempster DW. A novel tetracycline labeling schedule for longitudinal evaluation of the short-term effects of anabolic therapy with a single iliac crest bone biopsy: early actions of teriparatide. *J Bone Miner Res.* 2006; 21:366–73. [PubMed: 16491283]
9. Pierroz DD, Bonnet N, Baldock PA, Ominsky MS, Stolina M, Kostenuik PJ, Ferrari SL. Are osteoclasts needed for the bone anabolic response to parathyroid hormone? A study of intermittent parathyroid hormone with denosumab or alendronate in knock-in mice expressing humanized RANKL. *J Biol Chem.* 2010; 285:28164–73. [PubMed: 20558734]
10. Altman AR, Tseng WJ, de Bakker CM, Huh BK, Chandra A, Qin L, Liu XS. A closer look at the immediate trabecula response to combined parathyroid hormone and alendronate treatment. *Bone.* 2014; 61C:149–157. [PubMed: 24468717]
11. Black DM, Greenspan SL, Ensrud KE, Palermo L, McGowan JA, Lang TF, Garnero P, Bouxsein ML, Bilezikian JP, Rosen CJ. The effects of parathyroid hormone and alendronate alone or in combination in postmenopausal osteoporosis. *N Engl J Med.* 2003; 349:1207–15. [PubMed: 14500804]
12. Cosman F, Eriksen EF, Recknor C, Miller PD, Guanabens N, Kasperk C, Papanastasiou P, Readie A, Rao H, Gasser JA, Bucci-Rechtweg C, Boonen S. Effects of intravenous zoledronic acid plus subcutaneous teriparatide [rhPTH(1-34)] in postmenopausal osteoporosis. *J Bone Miner Res.* 2011; 26:503–11. [PubMed: 20814967]
13. Finkelstein JS, Hayes A, Hunzelman JL, Wyland JJ, Lee H, Neer RM. The effects of parathyroid hormone, alendronate, or both in men with osteoporosis. *N Engl J Med.* 2003; 349:1216–26. [PubMed: 14500805]
14. Finkelstein JS, Wyland JJ, Lee H, Neer RM. Effects of teriparatide, alendronate, or both in women with postmenopausal osteoporosis. *J Clin Endocrinol Metab.* 2010; 95:1838–45. [PubMed: 20164296]
15. Muschitz C, Kocijan R, Fahrleitner-Pammer A, Lung S, Resch H. Antiresorptives overlapping ongoing teriparatide treatment result in additional increases in bone mineral density. *J Bone Miner Res.* 2013; 28:196–205. [PubMed: 22836585]
16. Cosman F, Keaveny TM, Kopperdahl D, Wermers RA, Wan X, Krohn KD, Krege JH. Hip and spine strength effects of adding versus switching to teriparatide in postmenopausal women with

- osteoporosis treated with prior alendronate or raloxifene. *J Bone Miner Res.* 2013; 28:1328–36. [PubMed: 23281041]
17. Cosman F, Nieves J, Zion M, Woelfert L, Luckey M, Lindsay R. Daily and cyclic parathyroid hormone in women receiving alendronate. *N Engl J Med.* 2005; 353:566–75. [PubMed: 16093465]
 18. Cosman F, Wermers RA, Recknor C, Mauck KF, Xie L, Glass EV, Krege JH. Effects of teriparatide in postmenopausal women with osteoporosis on prior alendronate or raloxifene: differences between stopping and continuing the antiresorptive agent. *J Clin Endocrinol Metab.* 2009; 94:3772–80. [PubMed: 19584192]
 19. Schafer AL, Burghardt AJ, Sellmeyer DE, Palermo L, Shoback DM, Majumdar S, Black DM. Postmenopausal women treated with combination parathyroid hormone (1-84) and ibandronate demonstrate different microstructural changes at the radius vs. tibia: the PTH and Ibandronate Combination Study (PICS). *Osteoporos Int.* 2013; 24:2591–601. [PubMed: 23589163]
 20. Tsai JN, Uihlein AV, Lee H, Kumbhani R, Siwila-Sackman E, McKay EA, Burnett-Bowie SA, Neer RM, Leder BZ. Teriparatide and denosumab, alone or combined, in women with postmenopausal osteoporosis: the DATA study randomised trial. *Lancet.* 2013; 382:50–6. [PubMed: 23683600]
 21. Amugongo SK, Yao W, Jia J, Lay YA, Dai W, Jiang L, Walsh D, Li CS, Dave NK, Olivera D, Panganiban B, Ritchie RO, Lane NE. Effects of sequential osteoporosis treatments on trabecular bone in adult rats with low bone mass. *Osteoporos Int.* 2014; 25:1735–50. [PubMed: 24722767]
 22. Goff MG, Slyfield CR, Kummari SR, Tkachenko EV, Fischer SE, Yi YH, Jekir MG, Keaveny TM, Hernandez CJ. Three-dimensional characterization of resorption cavity size and location in human vertebral trabecular bone. *Bone.* 2012; 51:28–37. [PubMed: 22507299]
 23. Matheny JB, Slyfield CR, Tkachenko EV, Lin I, Ehlert KM, Tomlinson RE, Wilson DL, Hernandez CJ. Anti-resorptive agents reduce the size of resorption cavities: a three-dimensional dynamic bone histomorphometry study. *Bone.* 2013; 57:277–83. [PubMed: 23988275]
 24. Slyfield CR, Tkachenko EV, Wilson DL, Hernandez CJ. Three-dimensional dynamic bone histomorphometry. *J Bone Miner Res.* 2012; 27:486–95. [PubMed: 22028195]
 25. Slyfield CR Jr, Niemeyer KE, Tkachenko EV, Tomlinson RE, Steyer GG, Patthanacharoenphon CG, Kazakia GJ, Wilson DL, Hernandez CJ. Three-dimensional surface texture visualization of bone tissue through epifluorescence-based serial block face imaging. *J Microsc.* 2009; 236:52–9. [PubMed: 19772536]
 26. Tkachenko EV, Slyfield CR, Tomlinson RE, Daggett JR, Wilson DL, Hernandez CJ. Voxel size and measures of individual resorption cavities in three-dimensional images of cancellous bone. *Bone.* 2009; 45:487–92. [PubMed: 19482097]
 27. Waarsing JH, Day JS, van der Linden JC, Ederveen AG, Spanjers C, De Clerck N, Sasov A, Verhaar JA, Weinans H. Detecting and tracking local changes in the tibiae of individual rats: a novel method to analyse longitudinal in vivo micro-CT data. *Bone.* 2004; 34:163–9. [PubMed: 14751574]
 28. Schulte FA, Lambers FM, Kuhn G, Muller R. In vivo micro-computed tomography allows direct three-dimensional quantification of both bone formation and bone resorption parameters using time-lapsed imaging. *Bone.* 2011; 48:433–42. [PubMed: 20950723]
 29. Lambers FM, Kuhn G, Schulte FA, Koch K, Muller R. Longitudinal assessment of in vivo bone dynamics in a mouse tail model of postmenopausal osteoporosis. *Calcif Tissue Int.* 2012; 90:108–19. [PubMed: 22159822]
 30. Lukas C, Ruffoni D, Lambers FM, Schulte FA, Kuhn G, Kollmannsberger P, Weinkamer R, Muller R. Mineralization kinetics in murine trabecular bone quantified by time-lapsed in vivo micro-computed tomography. *Bone.* 2013; 56:55–60. [PubMed: 23684803]
 31. Schulte FA, Ruffoni D, Lambers FM, Christen D, Webster DJ, Kuhn G, Muller R. Local mechanical stimuli regulate bone formation and resorption in mice at the tissue level. *PLoS One.* 2013; 8:e62172. [PubMed: 23637993]
 32. Li M, Shen Y, Qi H, Wronski TJ. Comparative study of skeletal response to estrogen depletion at red and yellow marrow sites in rats. *Anat Rec.* 1996; 245:472–80. [PubMed: 8800405]

33. Hansson LI, Menander-Sellman K, Stenstrom A, Thorngren KG. Rate of normal longitudinal bone growth in the rat. *Calcif Tissue Res.* 1972; 10:238–51. [PubMed: 4639288]
34. Lan S, Luo S, Huh BK, Chandra A, Altman AR, Qin L, Liu XS. 3D image registration is critical to ensure accurate detection of longitudinal changes in trabecular bone density, microstructure, and stiffness measurements in rat tibiae by in vivo microcomputed tomography (muCT). *Bone.* 2013; 56:83–90. [PubMed: 23727434]
35. Altman, AR.; Tseng, WJ.; Chandra, A.; Qin, L.; Liu, XS. American Society of Bone and Mineral Research Annual Meeting. Houston, TX: 2014. Intermittent Parathyroid Hormone Treatment Enhances Both Trabecular and Cortical Bone Modeling in Growing Rats..
36. Chandra A, Lan S, Zhu J, Lin T, Zhang X, Siclari VA, Altman AR, Cengel KA, Liu XS, Qin L. PTH prevents the adverse effects of focal radiation on bone architecture in young rats. *Bone.* 2013; 55:449–57. [PubMed: 23466454]
37. Johnson, HJ.; McCormick, M.; Ibanez, L.; Consortium, IS. The ITK Software Guide. 2013.
38. Guo XE, Goldstein SA. Is trabecular bone tissue different from cortical bone tissue? *Forma.* 1997; 12:185–196.
39. Hollister SJ, Brennan JM, Kikuchi N. A homogenization sampling procedure for calculating trabecular bone effective stiffness and tissue level stress. *J Biomech.* 1994; 27:433–44. [PubMed: 8188724]
40. Parfitt AM, Drezner MK, Glorieux FH, Kanis JA, Malluche H, Meunier PJ, Ott SM, Recker RR. Bone histomorphometry: standardization of nomenclature, symbols, and units. Report of the ASBMR Histomorphometry Nomenclature Committee. *J Bone Miner Res.* 1987; 2:595–610. [PubMed: 3455637]
41. Johnston S, Andrews S, Shen V, Cosman F, Lindsay R, Dempster DW, Iida-Klein A. The effects of combination of alendronate and human parathyroid hormone(1-34) on bone strength are synergistic in the lumbar vertebra and additive in the femur of C57BL/6J mice. *Endocrinology.* 2007; 148:4466–74. [PubMed: 17569757]
42. Ma YL, Bryant HU, Zeng Q, Schmidt A, Hoover J, Cole HW, Yao W, Jee WS, Sato M. New bone formation with teriparatide [human parathyroid hormone-(1-34)] is not retarded by long-term pretreatment with alendronate, estrogen, or raloxifene in ovariectomized rats. *Endocrinology.* 2003; 144:2008–15. [PubMed: 12697709]
43. Samadfam R, Xia Q, Goltzman D. Co-treatment of PTH with osteoprotegerin or alendronate increases its anabolic effect on the skeleton of oophorectomized mice. *J Bone Miner Res.* 2007; 22:55–63. [PubMed: 17014384]
44. Samadfam R, Xia Q, Goltzman D. Pretreatment with anticatabolic agents blunts but does not eliminate the skeletal anabolic response to parathyroid hormone in oophorectomized mice. *Endocrinology.* 2007; 148:2778–87. [PubMed: 17379647]
45. Bilezikian JP. Combination anabolic and antiresorptive therapy for osteoporosis: opening the anabolic window. *Curr Osteoporos Rep.* 2008; 6:24–30. [PubMed: 18430397]
46. Brouwers JE, van Rietbergen B, Huiskes R. No effects of in vivo micro-CT radiation on structural parameters and bone marrow cells in proximal tibia of wistar rats detected after eight weekly scans. *J Orthop Res.* 2007; 25:1325–32. [PubMed: 17568420]
47. Wang Q, Seeman E. Skeletal growth and peak bone strength. *Best Pract Res Clin Endocrinol Metab.* 2008; 22:687–700. [PubMed: 19028352]
48. Wang Q, Wang XF, Iuliano-Burns S, Ghasem-Zadeh A, Zebaze R, Seeman E. Rapid growth produces transient cortical weakness: a risk factor for metaphyseal fractures during puberty. *J Bone Miner Res.* 2010; 25:1521–6. [PubMed: 20200962]

Highlights

- A μ CT-based, *in vivo* dynamic bone histomorphometry technique was developed to longitudinally quantify trabecular bone remodeling in rat tibiae.
- The μ CT-based bone formation and resorption rate correlate highly with traditional measures of bone formation and resorption.
- Combination therapy of PTH and ALN increased bone formation while inhibiting resorption.
- Results suggest that bone's early response to PTH may follow a resorption-independent pathway.

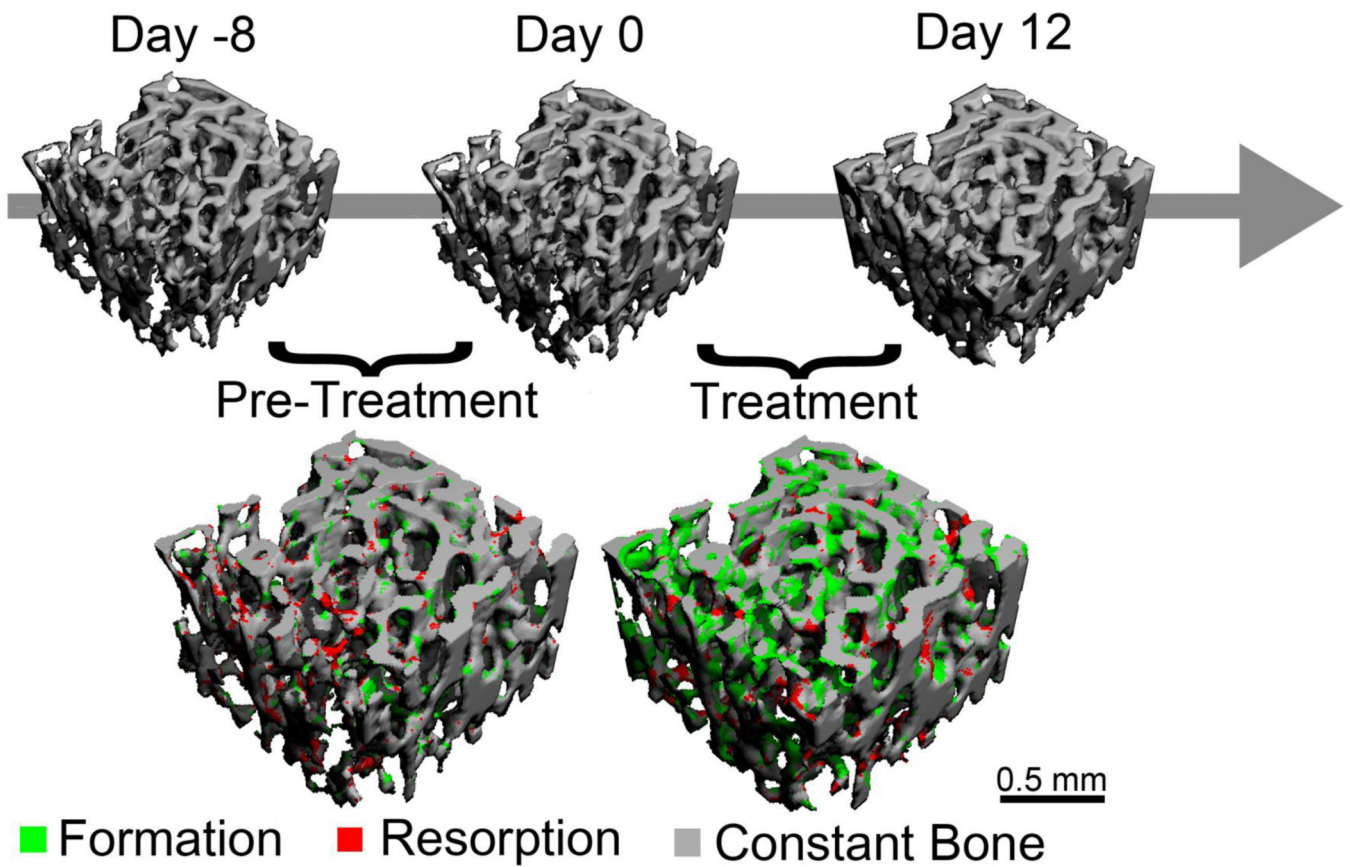


Figure 1.

Overview of the study design: Rats were scanned on days 0 and 12, and the 3D *in vivo* dynamic bone histomorphometry technique was applied to identify regions of bone formation (green) and resorption (red). A subset of rats was also scanned at day -8 to allow for a pre-treatment measure of bone remodeling.

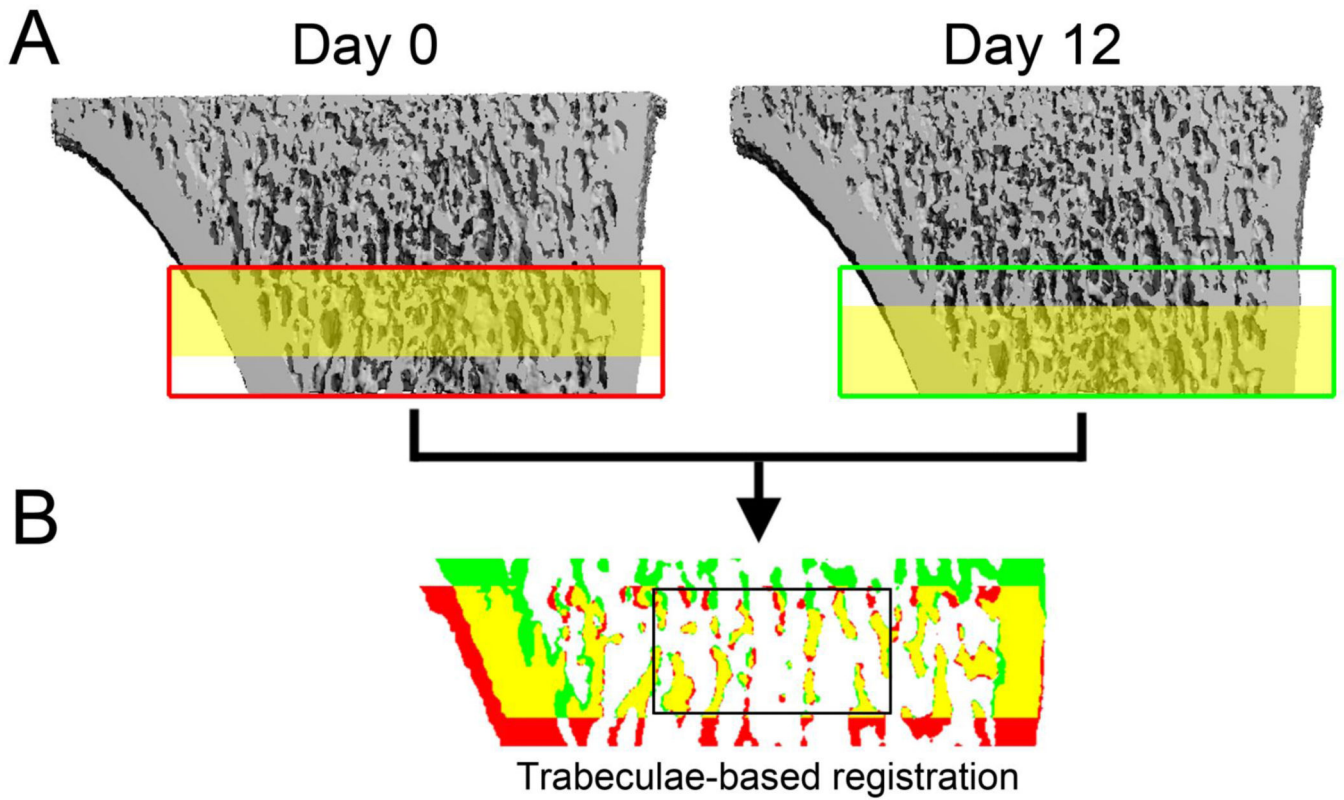


Figure 2.

Images were aligned through a multi-step registration procedure: (A) Initial registration based on the cortex resulted in similar orientation of the two scans, but the same trabecular pattern (shaded yellow) was offset between the two images. (B) After a trabeculae-specific registration, the trabeculae were precisely aligned between the two scans, allowing the identification of bone present only in the day 0 image (red), bone present in the day 12 image (green) and overlapped bone present in both images (yellow). This allowed the effects of trabecular remodeling within the representative VOI (outlined in black) to be delineated from those of linear growth.

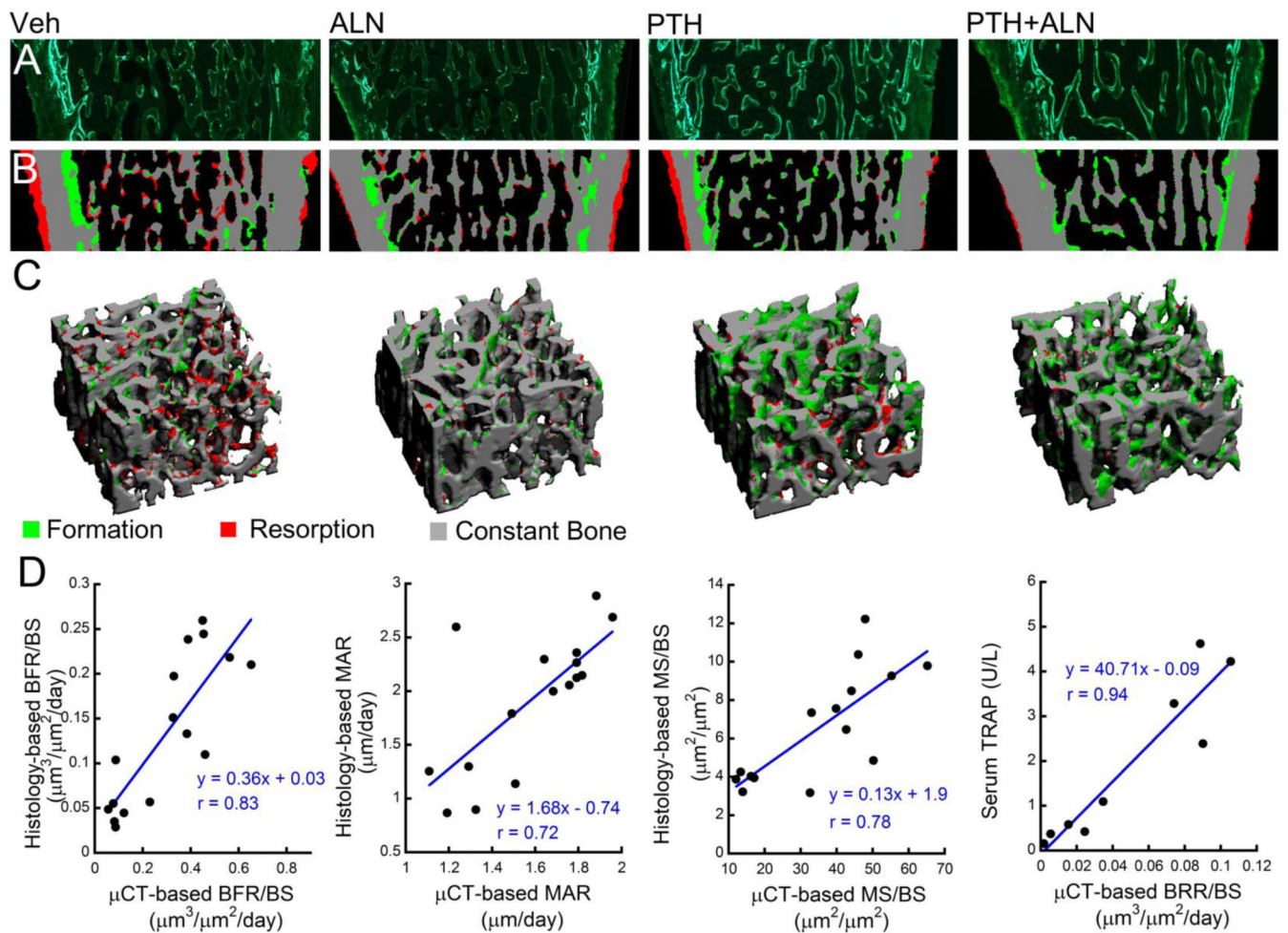


Figure 3.

Validation of *in vivo* dynamic histomorphometry technique: Paired comparisons were made between regions of bone formation identified through (A) traditional calcein-labeled histology and (B) μCT -based *in vivo* dynamic bone histomorphometry. (C) A VOI from the μCT image was selected and (D) BFR/BS, MAR, MS/BS, and BRR/BS were calculated based on the μCT images and correlated with traditional dynamic histomorphometry and serum TRAP.

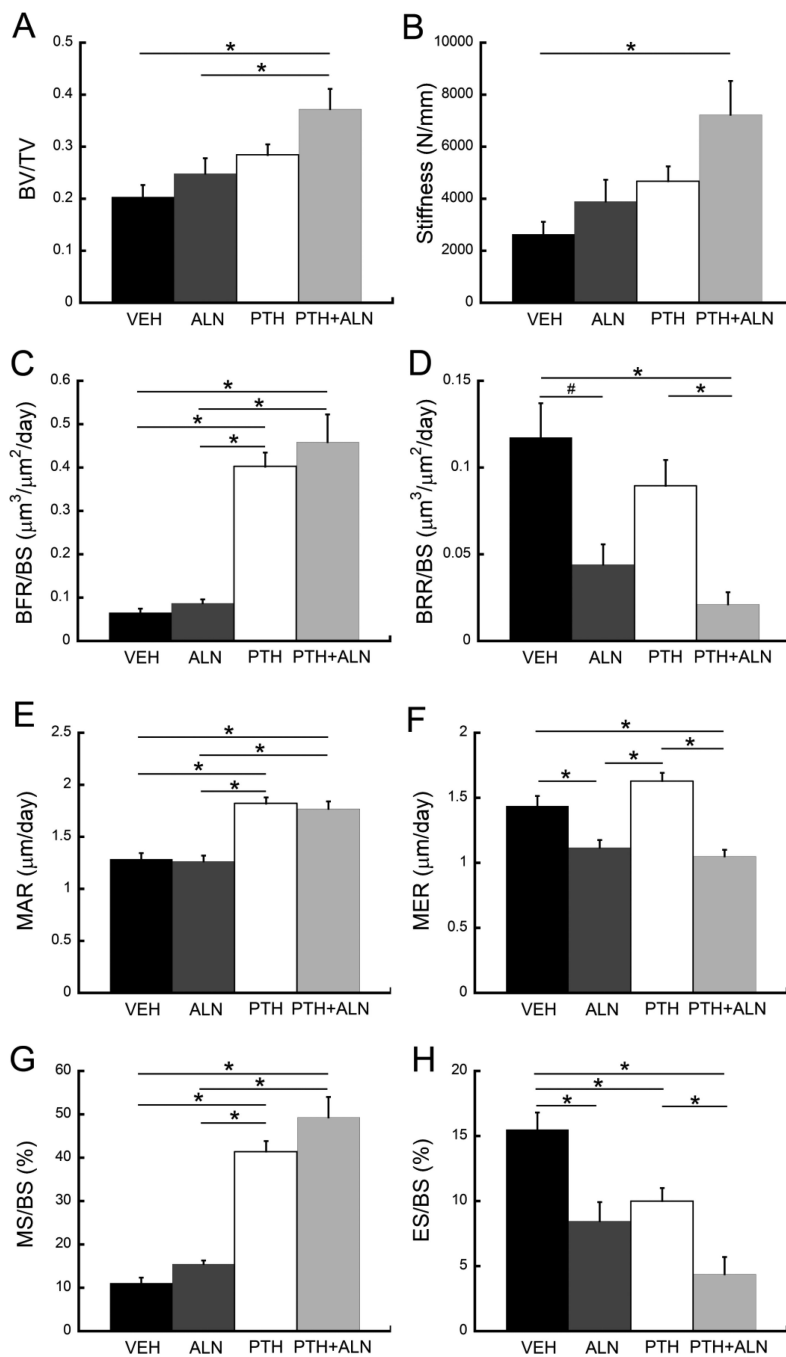


Figure 4. Comparisons among treatment groups in (A) BV/TV, (B) trabecular stiffness, (C) BFR/BS, (D) BRR/BS, (E) MAR, (F) MER, (G) MS/BS, and (H) ES/BS. *: $p < 0.05$

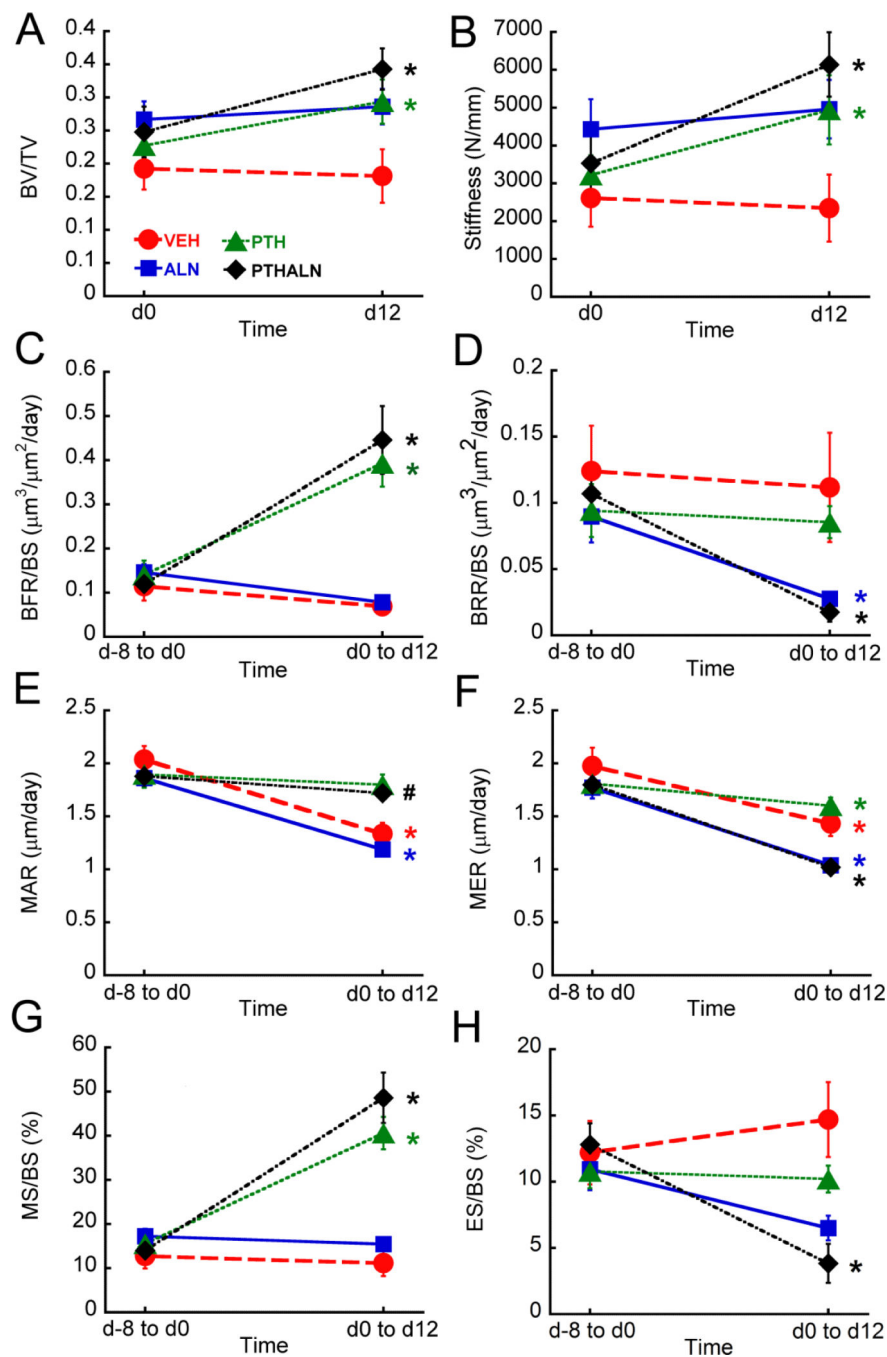


Figure 5. Longitudinal changes in (A) BV/TV, (B) trabecular stiffness, (C) BFR/BS, (D) BRR/BS, (E) MAR, (F) MER, (G) MS/BS, and (H) ES/BS. *: $p < 0.05$, #: $p < 0.1$

Table 1

Measurements based on traditional static and dynamic histology and serum marker TRAP. Values are shown as mean \pm SEM.

	VEH	ALN	PTH	PTH+ALN
BFR/BS ($\mu\text{m}^3/\mu\text{m}^2/\text{day}$)	$0.049 \pm 0.012^{c,d}$	$0.052 \pm 0.013^{c,d}$	$0.218 \pm 0.019^{a,b}$	$0.180 \pm 0.021^{a,b}$
MAR ($\mu\text{m}/\text{day}$)	$1.17 \pm 0.15^{c,d}$	$1.35 \pm 0.32^{c,d}$	$2.48 \pm 0.15^{a,b}$	$2.11 \pm 0.054^{a,b}$
MS/BS ($\mu\text{m}^2/\mu\text{m}^2$)	$0.040 \pm 0.006^{c,d}$	$0.038 \pm 0.001^{c,d}$	$0.088 \pm 0.009^{a,b}$	$0.084 \pm 0.009^{a,b}$
TRAP (U/L)	2.29 ± 0.61	0.70 ± 0.20^c	$3.60 \pm 0.60^{b,d}$	0.40 ± 0.14^c
Ob.N/BS ($1/\mu\text{m}^2$)	8.92 ± 0.66^c	5.58 ± 0.31^c	$15.09 \pm 1.37^{a,b}$	10.15 ± 1.28
Oc.N/BS ($1/\mu\text{m}^2$)	1.38 ± 0.11	0.66 ± 0.27^c	$1.47 \pm 0.15^{b,d}$	0.80 ± 0.13^c
Ob.S/BS ($\mu\text{m}^2/\mu\text{m}^2$)	$0.139 \pm 0.010^{c,d}$	$0.132 \pm 0.013^{c,d}$	$0.288 \pm 0.029^{a,b}$	$0.277 \pm 0.022^{a,b}$
Oc.S/BS ($\mu\text{m}^2/\mu\text{m}^2$)	0.071 ± 0.008	0.056 ± 0.025	0.087 ± 0.008	0.060 ± 0.008

^a significantly different from VEH

^b significantly different from ALN

^c significantly different from PTH

^d significantly different from PTH+ALN, $p < 0.05$